Random First Order Transition Theory for Glassy Dynamics in a Single Condensed Polymer

Hyun Woo Cho,[1,2] Guang Shi,[1] T. R. Kirkpatrick,[3] and D. Thirumalai[1]
[1]Department of Chemistry, University of Texas at Austin, Austin, Texas 78712, USA
[2]Department of Fine Chemistry, Seoul National University of Science and Technology, Seoul 01811, Korea
[3]Institute for Physical Science and Technology, University of Maryland, College Park, Maryland 20742, USA

(Received 10 September 2020; revised 21 December 2020; accepted 1 March 2021; published 2 April 2021)

The number of compact structures of a single condensed polymer (SCP), with similar free energies, grows exponentially with the degree of polymerization. In analogy with structural glasses (SGs), we expect that at low temperatures chain relaxation should occur by activated transitions between the compact metastable states. By evolving the states of the SCP, linearly coupled to a reference state, we show that, below a dynamical transition temperature (T_d), the SCP is trapped in a metastable state leading to slow dynamics. At a lower temperature, $T_K \neq 0$, the configurational entropy vanishes, resulting in a thermodynamic random first order ideal glass transition. The relaxation time obeys the Vogel-Fulcher-Tamman law, diverging at $T = T_0 \approx T_K$. These findings, accord well with the random first order transition theory, establishing that SCP and SG exhibit similar universal characteristics.

DOI: 10.1103/PhysRevLett.126.137801

Experiments suggest that glasslike behavior should be expected in chromosome dynamics [1–3], collapse kinetics of polymers [4], and intrinsically disordered proteins [5]. Dynamics [6–8], and phase behavior [9–11] of single polymers exhibit glassy behavior upon cooling or compression [12–14]. However, it is unknown whether the glass transition in a single polymer is governed by the same physical principles that describe their macroscopic counterparts.

Single condensed polymer (SCP) should exhibit glasslike behavior because their phase space structure satisfies all the requirements for observing slow dynamics. At temperature (T) below the coil-to-globule temperature T_θ the number of compact structures or states, with similar free energies, scales exponentially with N [15]. At low T transition between compact structures can only occur by activated transitions. Because the physical picture for a SCP is the same as in the structural glass transition (SGT), the dynamics of the SCP should be described by theories developed for bulk glassy systems. We anticipate that the SCP dynamics, over a wide range of temperatures, can be understood within the framework of the random first order transition (RFOT) theory. That this is so is the main conclusion of this work.

Let us describe the salient aspects of the energy landscape of the SCP and liquids that undergo the SGT. The SGT dynamics is well described by the RFOT theory [16], based on spin glass models [17–19]. An ingredient in the RFOT theory for the SGT is the emergence of an exponentially large number of metastable states [20] below the dynamic transition temperature, T_d [17,18]. The free energy barrier $\Delta F^\ddagger$ between the metastable states is related to the configurational entropy, $S_{\rm conf}$ as $\Delta F^\ddagger \sim S_{\rm conf}^{-1}$ [16]. Since $S_{\rm conf}$ decreases as T decreases, $\Delta F^\ddagger$ increases, resulting in a significant increase in the structural relaxation time. RFOT theory predicts that $S_{\rm conf}$ vanishes at an ideal glass transition temperature, $T_K < T_d$, at which a thermodynamic random first-order transition, without latent heat, occurs from a supercooled liquid to an ideal glass.

To affirm the predictions of the RFOT theory in the SCP, we use the Franz-Parisi (FP) method [21,22], which involves coupling two copies of the system through a field with strength ϵ. FP showed [23–27] that an order parameter, measuring the structural similarity between the states, exhibited first order transition at nonzero ϵ only when a large number of metastable states emerge.

We used a bead-spring model [28] for a polymer with $N = 128$ weakly attractive Lennard-Jones (LJ) particles linearly connected by a harmonic potential (Sec. I of the Supplemental Material [29]). Parameters of the potentials are chosen to suppress crystallization (Sec. II of Ref. [29]). The model in which solvent effects are implicitly taken into account by varying the strength of the interaction between the monomers captures the universal dynamic and static properties of polymeric systems [37]. We adopted this well-tested approach to investigate universal aspect of glass formation in a single condensed polymer. Surprisingly, minimal models quantitatively reproduce the scattering profiles of disordered proteins [38]. These observations justify the polymer model used here.

Following FP (Fig. 1), we created two replicas of the SCP at the same T. Replica 1 in Fig. 1 is a fixed reference conformation ($\{\vec{r}_0\}$), chosen from an equilibrium ensemble, and serves as a quenched random field. The conformation of $\{\vec{r}\}$ in replica 2 (Fig. 1) is evolved using

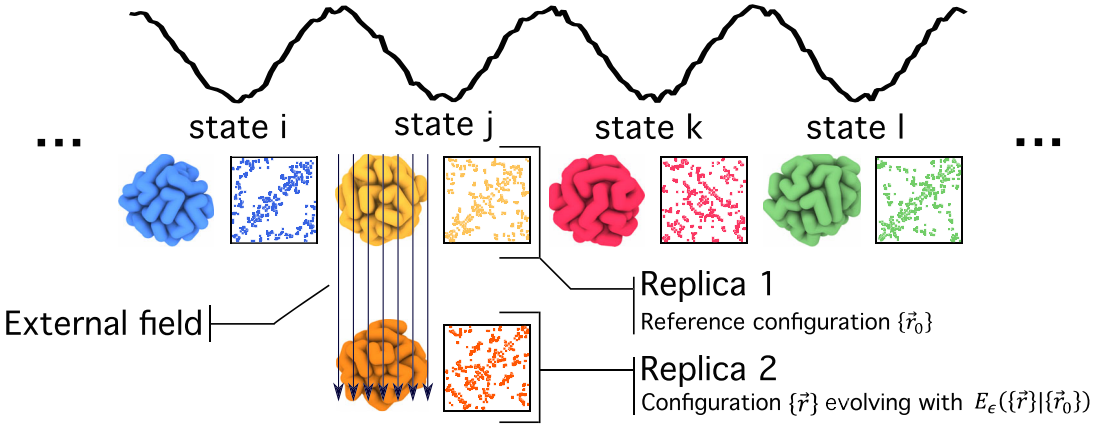

FIG. 1. Implementation of the Franz-Parisi method. The equilibrium conformation in replica 1 is one of the exponentially large number of metastable sates, which is coupled to replica 2. The panels next to the snapshot are the contact maps in the metastable states. The overlap between replicas 1 and 2 measures the static structural similarity (blue and red, for example).

Monte Carlo simulation by coupling it to replica 1 (Fig. 1). The energy $E_\epsilon(\{\vec{r}\}|\{\vec{r}_0\})$ of the coupled replicas is

$$E_\epsilon(\{\vec{r}\}|\{\vec{r}_0\}) = E(\{\vec{r}\}) - N\epsilon\hat{Q}_{\rm stat}(\{\vec{r}\},\{\vec{r}_0\}), \quad (1)$$

where $E(\{\vec{r}\})$ is the potential energy of the SCP in replica 2, ϵ is the strength of the external field, and $\hat{Q}_{\rm stat}(\{\vec{r}\},\{\vec{r}_0\})$ measures the static structural similarity between $\{\vec{r}\}$ and $\{\vec{r}_0\}$.

We used contact maps, two-dimensional representations of a given structure of the SCP, to calculate $\hat{Q}_{\rm stat}$. Two noncovalently linked monomers are in contact if the distance between them is less than $R_c = 1.4\sigma$, the first minimum in the radial distribution function (Sec. II in the Supplemental Material [29]). Panels next to the snapshots in Fig. 1 are examples of the contact maps.

The static overlap function $\hat{Q}_{\rm stat}$ is calculated using

$$\hat{Q}_{\rm stat}(\{\vec{r}\},\{\vec{r}_0\}) = \frac{\sum_{(i,j)'} q_{ij}(\{\vec{r}\})q_{ij}(\{\vec{r}_0\})}{\sum_{(i,j)'} q_{ij}(\{\vec{r}_0\})}, \quad (2)$$

where $q_{ij}(\{\vec{r}\})$ is the contact function. It is unity if i and j monomers are in contact and zero otherwise, and $(i,j)'$ is the sum over all nonbonded pairs of monomers. The average of the static order parameter $\langle\hat{Q}_{\rm stat}\rangle$ was obtained by taking a Boltzmann-weighted average over $\vec{r}$ and $\vec{r}_0$; we first performed a *thermal* average of $\hat{Q}_{\rm stat}$ with $\{\vec{r}_0\}$ fixed, and then a *disorder* average over various $\{\vec{r}_0\}$ was calculated to account for the fluctuations caused by differences in $\{\vec{r}_0\}$ (details are in Sec. I of the Supplemental Material [29] and the relation to the random field Ising model is given in Sec. V). If $\{\vec{r}\}$ and $\{\vec{r}_0\}$ are identical, $\hat{Q}_{\rm stat}(\{\vec{r}\},\{\vec{r}\}) = 1$, resulting in $\langle\hat{Q}_{\rm stat}\rangle = 1$. If the replicas are totally uncorrelated, $\langle\hat{Q}_{\rm stat}\rangle$ is the average contact probability $\langle q_{ij}\rangle$, which is $\simeq$0.13 for the parameters used in the simulations. From Eqs (1) and (2), it follows that $Q_{\rm stat}$ varies as a function of ϵ. When the external field strength ϵ is sufficiently large, $\{\vec{r}\}$ is biased to $\{\vec{r}_0\}$, such that $\langle\hat{Q}_{\rm stat}\rangle \simeq 1$. If ϵ decreases to 0, $\{\vec{r}\}$ is independent of $\{\vec{r}_0\}$, resulting in $\langle\hat{Q}_{\rm stat}\rangle \simeq \langle q_{ij}\rangle$.

The changes in $\langle\hat{Q}_{\rm stat}\rangle$ with $\epsilon \neq 0$ should have the characteristics of first order transition only if metastable states are probed. Since all the metastable states are generated at the same thermodynamic condition (the same T and N), they are equivalent. The individual free energy of metastable α is F_α. The canonical free energy $F_{\rm tot}$ is less than the component averaged free energy, $\sum_\alpha P_\alpha F_\alpha$, where P_α is the probability of being in the state α [16,39,40]. The difference between the two is $TS_{\rm conf}$, the entropic gain arising from an exploration of all possible states, $F_{\rm tot} = F_\alpha - TS_{\rm conf}$. Thus, if ϵ is strong enough to compensate for the entropic penalty, the SCP in replica 2 would be trapped in a single metastable state, such that $\langle\hat{Q}_{\rm stat}\rangle = Q_{\rm glass} \simeq 1$. Otherwise, it could explore all possible metastable states over time, resulting in $\langle\hat{Q}_{\rm stat}\rangle$ equalling $Q_{\rm liquid} = \langle q_{ij}\rangle$. Thus, at the critical value of $\epsilon = \epsilon_c$ where $N\epsilon_c(Q_{\rm glass} - Q_{\rm liquid}) \simeq TS_{\rm conf}$, $\langle\hat{Q}_{\rm stat}\rangle$ should change discontinuously between $Q_{\rm glass}$ and $Q_{\rm liquid}$, which would be a signature of a first order transition. By showing $\hat{Q}_{\rm stat}$ exhibits the first-order-like transition at $\epsilon \neq 0$, we can confirm the existence of metastable states in the SCP.

In the upper panel of Fig. 2(a), $\langle\hat{Q}_{\rm stat}\rangle$ is plotted as a function of ϵ for various T (the open symbols). As expected, $\langle\hat{Q}_{\rm stat}\rangle$ decreases from $\simeq$1 to $\langle q_{ij}\rangle \simeq 0.13$ as ϵ decreases to 0. The static susceptibility, $\chi_{\rm stat}(\epsilon) = N(\langle\hat{Q}^2_{\rm stat}\rangle - \langle\hat{Q}_{\rm stat}\rangle^2)$, has a peak at the value of ϵ where $\langle\hat{Q}_{\rm stat}\rangle$ changes drastically [the dashed vertical lines in Fig. 2(a)]. The width of the peaks decreases and the amplitudes increase as T decreases, reflecting a sharp change in $\langle\hat{Q}_{\rm stat}\rangle$ at T. Such sharp changes in $\langle\hat{Q}_{\rm stat}\rangle$ and $\chi_{\rm stat}(\epsilon)$ provide evidence for the first-order-like phase transition in the presence of the coupling field. We establish in Sec. III of the Supplemental Material [29] that the first order nature of the transition is more pronounced as N increases.

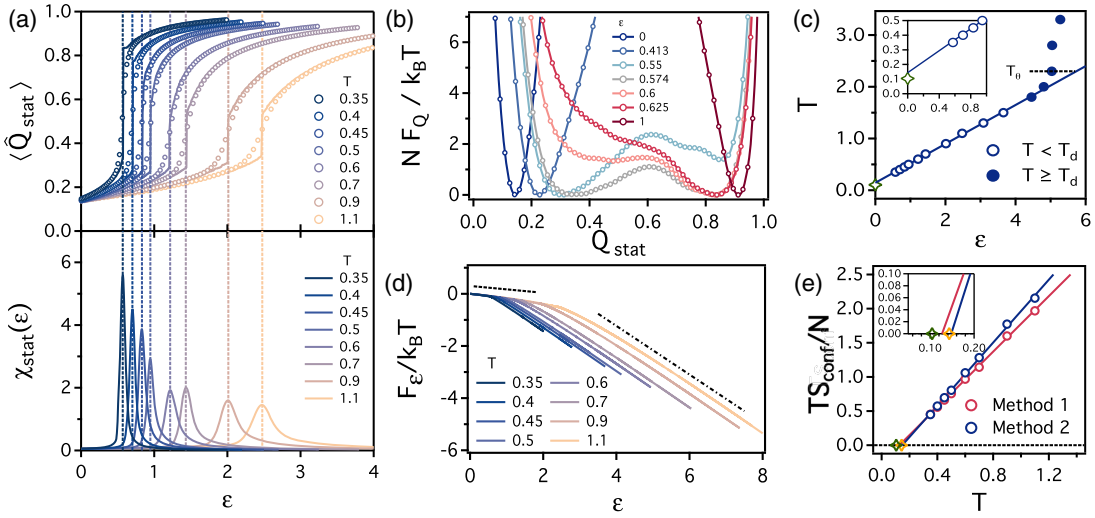

FIG. 2. Phase behavior of $\hat{Q}_{\rm stat}$. (a) Average $\langle \hat{Q}_{\rm stat} \rangle$ (the upper panel) and susceptibility $\chi_{\rm stat}(\epsilon)$ (the lower panel) of the order parameters with respect to ϵ for various T. The vertical dashed lines are the positions of ϵ where $\chi_{\rm stat}(\epsilon)$ has the maximum value. The solid lines represent the position of $Q_{\rm stat}$, where F_Q in (b) has the minimum value. (b) F_Q for various ϵ at $T = 0.35$. F_Q in the graph is shifted by its minimum value. (c) $T - \epsilon$ phase diagram of $\hat{Q}_{\rm stat}$. The open and filled symbols represent T of ϵ_c for $T < T_d$ and $T \geq T_d$, respectively. The solid line is a linear fit for $T < T_d$. The black dashed line denotes the position of T_θ. The open green star denotes T_0. The inset is the same phase diagram at $0 \leq \epsilon \leq 0.9$. (d) F_ϵ as a function of ϵ for various T. F_ϵ is shifted by $F_{\epsilon=0}$. The slopes of the dashed and dashed-dotted lines are -0.13 and -0.93, respectively. (e) $TS_{\rm conf}/N$ as a function of T. The solid lines are linear fits. The yellow and green open symbols represent the T_0 and y intercept of the solid line in (c), respectively. In the inset, we magnify the graph near the x intercepts of the linear fits.

Next, we confirm that the abrupt change in $\langle \hat{Q}_{\rm stat} \rangle$ reflects a regular first order transition. In the first order transition, the minimum in the free energy F_Q as a function of $\hat{Q}_{\rm stat}$ changes discontinuously at the phase transition point. The free energy, F_Q, is calculated from the distribution $P(Q_{\rm stat}|\{\vec{r}_0\}) = \langle \delta(Q_{\rm stat} - \hat{Q}_{\rm stat}(\{\vec{r}\},\{\vec{r}_0\})) \rangle_T$, i.e., $-NF_Q/k_BT = \langle \ln P(Q_{\rm stat}|\{\vec{r}_0\}) \rangle_D$ [41], where $\langle \cdots \rangle_T$ and $\langle \cdots \rangle_D$ are the thermal and disorder averages of the property, respectively (see the definitions of $P(Q_{\rm stat}|\{\vec{r}_0\})$, $\langle \cdots \rangle_T$, and $\langle \cdots \rangle_D$ in Sec. I of the Supplemental Material [29]). In Fig. 2(b), F_Q at $T = 0.35$ is plotted as a function of $Q_{\rm stat}$ for various ϵ. When $\epsilon = 1$, F_Q has minimum at $Q_{\rm stat} \simeq 0.93$, indicating that $\{\vec{r}\}$ is pinned around the state associated with $\{\vec{r}_0\}$. As ϵ decreases to 0, the minimum shifts to $Q_{\rm stat} = 0.13$. At $\epsilon = 0.574$, where $\chi_{\rm stat}$ has a maximum, F_Q has two minima at $Q_{\rm stat} \approx 0.34$ and $Q_{\rm stat} \approx 0.84$. The two different states coexist at $\epsilon = 0.574$, which leads to a discontinuous change in the order parameter. In Fig. 2(a), we plotted the minimum position of F_Q as a function of ϵ for various T (the solid lines). The minimum position changes discontinuously at ϵ where the fluctuation in $\hat{Q}_{\rm stat}$ is maximized, revealing the first order nature of the transition.

We arrive at the same conclusion from the Ehrenfest classification, according to which $dF_\epsilon/d\epsilon$ should be discontinuous at the transition point. Here, F_ϵ is the free energy as a function of ϵ, which is calculated from F_Q using the Legendre transformation, $F_\epsilon = F_Q - \epsilon \langle \hat{Q}_{\rm stat} \rangle$, where ϵ is equal to $\epsilon = \partial F_Q/\partial Q_{\rm stat}$ [42]. Figure 2(d), displaying F_ϵ as a function of ϵ at various T, shows a discontinuous change in the slopes ($= dF_\epsilon/d\epsilon$) between -0.13 and -0.93 (the dashed and dashed-dotted lines, respectively), a signature of the first order transition. Since $\langle \hat{Q}_{\rm stat} \rangle = -dF_\epsilon/d\epsilon$, we define the effective order parameters in the two states as $Q_{\rm liquid} = 0.13$ and $Q_{\rm glass} = 0.93$. Thus, the discontinuous change in the slope in Fig. 2(d) corresponds to the discontinuous change in $\langle \hat{Q}_{\rm stat} \rangle$ between $Q_{\rm liquid}$ and $Q_{\rm glass}$. Figures 2(b) and 2(d) confirm that the first order transition in $\hat{Q}_{\rm stat}$ occurs with a change in ϵ, thus verifying the existence of the metastable states in the SCP.

RFOT theory predicts that the metastable states, separated by barriers, should cease to exist above the dynamical transition temperature T_d, which implies that the first-order transition nature of $\hat{Q}_{\rm stat}$ should disappear at $T > T_d$. We found that $\langle \hat{Q}_{\rm stat} \rangle$ changes continuously with ϵ when $T \geq 1.8$ (see Sec. IV of the Supplemental Material [29]). The coil-to-globule temperature is $T_\theta = 2.3 > T_d$ (Sec. II in Ref. [29]). Thus, the equilibrium collapse occurs before the dynamical transition, implying that the dynamics of the SCP in the temperature $T_d \leq T \leq T_\theta$ can be described by the standard polymer theory. Only below T_d the dynamics is determined by activated transitions between equivalent compact structures.

The phase behavior in Fig. 2(a) is summarized in Fig. 2(c). The phase boundaries (ϵ_c, T_c) are associated with the peak in $\chi_{\rm stat}$ at a given T (the open symbols in the graph). At $T < T_d$ (the open symbols), $\langle \hat{Q}_{\rm stat} \rangle$ changes discontinuously, and when $T > T_d$ (the filled triangles), it

changes continuously. Above T_θ (the black dashed line), ϵ_c is less dependent on T. Because T_c changes linearly with ϵ_c (when $T < T_d$), we extrapolate the phase boundary to $\epsilon = 0$ (the blue solid line). The y intercept in the linear fit is T_c at $\epsilon = 0$, which has a positive value at $\epsilon = 0$ [$T_c(\epsilon = 0) = 0.14$]. This signals that a thermodynamic transition would occur at the nonzero temperature when $\epsilon = 0$, implying that the free energy of individual metastable states F_α is equal to the total free energy $F_{\rm tot}$ at a finite temperature even without external fields, which is only possible if $S_{\rm conf} = 0$ at $T_c(\epsilon = 0)$.

We investigated if $S_{\rm conf}$ vanishes at $T_c(\epsilon = 0)$. Using two methods [26,41], $S_{\rm conf}$ at $\epsilon = 0$ is estimated as a function of T. Since the first order transition occurs when the entropic gain ($TS_{\rm conf}$) is compensated by the energetic contribution of the fields [$N\epsilon_c(Q_{\rm glass} - Q_{\rm liquid})$], we estimated the configurational entropy using (method 1) [26], $TS_{\rm conf}/N = \epsilon_c[Q_{\rm glass} - Q_{\rm liquid}]$. A more natural way is to calculate $TS_{\rm conf}$ as the difference between F_α and $F_{\rm tot}$, corresponding to $F_{Q_{\rm glass}}$ and $F_{Q_{\rm liquid}}$ at $\epsilon = 0$, respectively. Thus, $S_{\rm conf}$ can also be calculated using (method 2),

$$TS_{\rm conf}/N = F_{Q_{\rm glass}}(\epsilon = 0) - F_{Q_{\rm liquid}}(\epsilon = 0). \quad (3)$$

Figure 2(e) shows $TS_{\rm conf}/N$ (the open symbols) as a function of T using methods 1 and 2. Linear extrapolation of $TS_{\rm conf}/N$ (the linear lines) shows that $S_{\rm conf}$ vanishes at a similar nonzero value of T, regardless of the method used. It should be emphasized that the numerical value of the temperature is consistent with $T_c(\epsilon = 0)$ (the open yellow star). This confirms that it is because the configurational entropy vanishes that the thermodynamic transition occurs at $T_c(\epsilon = 0)$.

What is the nature of the thermodynamic transition at $T_c(\epsilon = 0)$? It corresponds to an ideal glass transition of the SCP. Most importantly, we note from Eq. (3), $TS_{\rm conf}$ is the energy difference between the two states, which accounts for the latent heat at the transition. Therefore, Fig. 2(e) shows that as T approaches $T_c(\epsilon = 0)$, the latent heat decreases and vanishes at $T_c(\epsilon = 0)$. This implies that at $T_c(\epsilon = 0)$, the SCP exhibits a *random* first order transition from liquid to an ideal glass without releasing latent heat but with a discontinuity in $\hat{Q}_{\rm stat}$. Hence, Figs. 2(c) and 2(e) show that the ideal glass transition in the SCP at $T_K = T_c(\epsilon = 0) \neq 0$ is truly the analog of T_K in bulk glasses.

There ought to be consistency between thermodynamic random first order transition and dynamics [43]. To investigate the dynamics of the SCP, we performed dynamic MC simulations (details in the Supplemental Material [29]). The time-dependent overlap function $Q_{\rm dyn}(t)$ is

$$Q_{\rm dyn}(t) = \frac{\sum_{(i,j)'} q_{ij}(t) q_{ij}(0)}{\sum_{(i,j)'} q_{ij}(0)}, \quad (4)$$

where $q_{ij}(t)$ is the contact function of a single polymer at time t; $Q_{\rm dyn}(t)$ quantifies how rapidly the contact map loses memory of the initial pattern. By definition $Q_{\rm dyn}(t = 0) = 1$. As $t \to \infty$, the SCP loses memory of the structural correlation, and thus the pattern of the contact map also becomes independent of the initial state. Consequently, $Q_{\rm dyn}(t)$ decays to $\langle q_{ij} \rangle$.

Figure 3(a) shows the time average of $Q_{\rm dyn}(t)$ ($\langle Q_{\rm dyn}(t) \rangle_t$) as a function of t at different T. As T decreases from 1.1 to 0.35, $\langle Q_{\rm dyn}(t) \rangle_t$ decays more slowly with the decay time constant increasing by a few orders of magnitude. Figure 3(b) shows that heights and timescales of the peak in the dynamic susceptibility, $\chi_{\rm dyn}(t) = N[\langle Q_{\rm dyn}(t)^2 \rangle_t - \langle Q_{\rm dyn}(t) \rangle_t^2]$, increase as T decreases, implying that the structural relaxation becomes heterogeneous as T decreases [44–46]. Figures 3(a) and 3(b) reveal that the sluggish structural relaxation in the SCP is accompanied by enhanced dynamic heterogeneity, an important dynamic property of glassy liquids [47,48].

The structural relaxation time τ_α [Fig. 3(c)], calculated using $\langle Q_{\rm dyn}(t = \tau_\alpha) \rangle_t = 0.3$, increases by more than 2 orders of magnitude when T decreases from 1.1 to 0.35 (the open symbols). The dramatic increase in τ_α in the SCP, metallic [49], colloidal systems [50], and molecular glasses [51], is described well by the Vogel-Fulcher-Tamman (VFT) equation, $\tau_\alpha = \tau_0 \exp[(D_0 T_0)/(T - T_0)]$, where τ_0, D_0, and T_0 are fitting parameters. We fit τ_α as a function of T to the VFT equation [the dashed line in Fig. 3(c)], yielding $T_0 = 0.1$, [the green open symbols in Figs. 2(c) and 2(e)]. The value of T_0 is close to T_K.

The divergence of τ_α is associated with a decrease in $S_{\rm conf}$ ($\ln \tau_\alpha \sim 1/TS_{\rm conf}$ [16]). Figure 3(d), showing $\ln \tau_\alpha$ as a

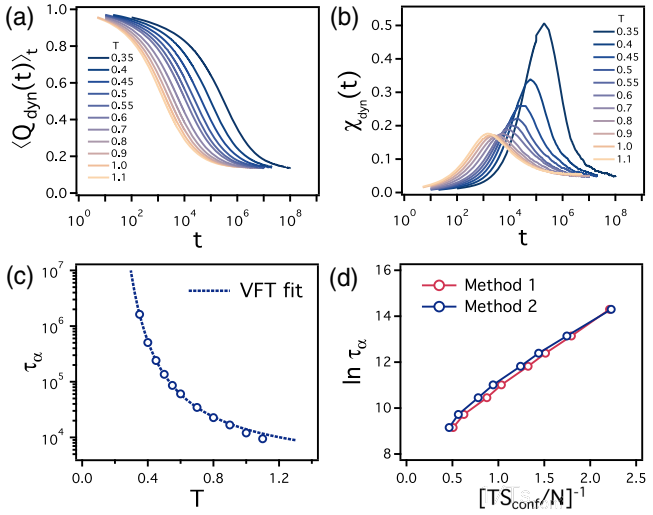

FIG. 3. Glassy dynamics in the SCP. (a) Time average of time dependent overlap function $\langle Q_{\rm dyn}(t) \rangle_t$ and (b) susceptibility $\chi_{\rm dyn}(t)$ for various T. (c) Dependence of τ_α on T (the open symbols). The dashed line is the VFT fit. (d) Relation between τ_α and $S_{\rm conf}$.

function of $[TS_{\mathrm{conf}}/N]^{-1}$, obtained using methods 1 and 2, shows that the increase in τ_α is closely related to the decrease in s_{conf}. Thus, the dynamics and statics of the SCP are consistent with RFOT predictions.

Our findings show that the RFOT theory holds for a diverse systems exhibiting changes from diffusive motion to activated transitions as a control parameter is changed. The requirement is the emergence of multiple metastable states, separated by free energy barriers, below a characteristic dynamical transition temperature. This feature is shared by the SCP and myriad glass forming systems, thus explaining the validity of the RFOT theory for condensed polymers.

This work was supported by NSF (CHE 19-00093), and the Welch Foundation Grant No. F-0019 through the Collie-Welch chair.

[1] I. Bronshtein, E. Kepten, I. Kanter, S. Berezin, M. Lindner, A. B. Redwood, S. Mai, S. Gonzalo, R. Foisner, Y. Shav-Tal *et al.*, Nat. Commun. **6**, 8044 (2015).
[2] E. H. Finn and T. Misteli, Science **365**, eaaw9498 (2019).
[3] H. Kang, Y.-G. Yoon, D. Thirumalai, and C. Hyeon, Phys. Rev. Lett. **115**, 198102 (2015).
[4] S. Kwon, H. W. Cho, J. Kim, and B. J. Sung, Phys. Rev. Lett. **119**, 087801 (2017).
[5] I. L. Morgan, R. Avinery, G. Rahamim, R. Beck, and O. A. Saleh, Phys. Rev. Lett. **125**, 058001 (2020).
[6] T. T. Perkins, S. R. Quake, D. E. Smith, and S. Chu, Science **264**, 822 (1994).
[7] F. Latinwo and C. M. Schroeder, Soft Matter **7**, 7907 (2011).
[8] M. V. Tamm, L. I. Nazarov, A. A. Gavrilov, and A. V. Chertovich, Phys. Rev. Lett. **114**, 178102 (2015).
[9] K. Yoshikawa, M. Takahashi, V. V. Vasilevskaya, and A. R. Khokhlov, Phys. Rev. Lett. **76**, 3029 (1996).
[10] F. Rampf, K. Binder, and W. Paul, J. Polym. Sci., Part B: Polym. Phys. **44**, 2542 (2006).
[11] M. P. Taylor, W. Paul, and K. Binder, J. Chem. Phys. **131**, 114907 (2009).
[12] N. V. Dokholyan, E. Pitard, S. V. Buldyrev, and H. E. Stanley, Phys. Rev. E **65**, 030801(R) (2002).
[13] M. Tress, E. U. Mapesa, W. Kossack, W. K. Kipnusu, M. Reiche, and F. Kremer, Science **341**, 1371 (2013).
[14] W. L. Merling, J. B. Mileski, J. F. Douglas, and D. S. Simmons, Macromolecules **49**, 7597 (2016).
[15] H. Orland, C. Itzykson, and C. de Dominicis, J. Phys. (Paris), Lett. **46**, L353 (1985).
[16] T. R. Kirkpatrick, D. Thirumalai, and P. G. Wolynes, Phys. Rev. A **40**, 1045 (1989).
[17] T. R. Kirkpatrick and D. Thirumalai, Phys. Rev. Lett. **58**, 2091 (1987).
[18] T. R. Kirkpatrick and D. Thirumalai, Phys. Rev. B **36**, 5388 (1987).
[19] T. R. Kirkpatrick and P. G. Wolynes, Phys. Rev. B **36**, 8552 (1987).
[20] M. Goldstein, J. Chem. Phys. **51**, 3728 (1969).
[21] S. Franz and G. Parisi, Phys. Rev. Lett. **79**, 2486 (1997).
[22] S. Franz and G. Parisi, J. Stat. Mech. (2013) P11012.
[23] L. Berthier, Phys. Rev. E **88**, 022313 (2013).
[24] G. Parisi and B. Seoane, Phys. Rev. E **89**, 022309 (2014).
[25] L. Berthier and R. L. Jack, Phys. Rev. Lett. **114**, 205701 (2015).
[26] L. Berthier and D. Coslovich, Proc. Natl. Acad. Sci. U.S.A. **111**, 11668 (2014).
[27] L. Berthier, P. Charbonneau, D. Coslovich, A. Ninarello, M. Ozawa, and S. Yaida, Proc. Natl. Acad. Sci. U.S.A. **114**, 11356 (2017).
[28] *Monte Carlo and Molecular Dynamics Simulations in Polymer Science*, 1st ed., edited by K. Binder (Oxford University Press, Oxford, 1996).
[29] See Supplemental Material at http://link.aps.org/supplemental/10.1103/PhysRevLett.126.137801 for details of the model and simulations, which includes Refs. [30–36].
[30] D. Frenkel and B. Smit, *Understanding Molecular Simulation: From Algorithms to Applications* (Elsevier, New York, 2001), Vol. 1.
[31] C. Bennemann, W. Paul, K. Binder, and B. Dünweg, Phys. Rev. E **57**, 843 (1998).
[32] D. F. Parsons and D. R. M. Williams, J. Chem. Phys. **124**, 221103 (2006).
[33] L. Berthier, G. Biroli, J.-P. Bouchaud, L. Cipelletti, D. El Masri, D. L'Hôte, F. Ladieu, and M. Pierno, Science **310**, 1797 (2005).
[34] L. Berthier, G. Biroli, J.-P. Bouchaud, W. Kob, K. Miyazaki, and D. R. Reichman, J. Chem. Phys. **126**, 184503 (2007).
[35] L. Berthier, G. Biroli, J.-P. Bouchaud, W. Kob, K. Miyazaki, and D. R. Reichman, J. Chem. Phys. **126**, 184504 (2007).
[36] D. S. Fisher, Phys. Rev. Lett. **56**, 416 (1986).
[37] M. Rubinstein and R. H. Colby, *Polymer Physics*, 1st ed. (Oxford University Press, Oxford, 2003).
[38] U. Baul, D. Chakraborty, M. L. Mugnai, J. E. Straub, and D. Thirumalai, J. Phys. Chem. B **123**, 3462 (2019).
[39] R. Palmer, Adv. Phys. **31**, 669 (1982).
[40] T. R. Kirkpatrick and D. Thirumalai, Rev. Mod. Phys. **87**, 183 (2015).
[41] L. Berthier, M. Ozawa, and C. Scalliet, J. Chem. Phys. **150**, 160902 (2019).
[42] M. Mézard and G. Parisi, *Glasses and Replicas* (John Wiley & Sons, New York, 2012), Chap. 4, pp. 151–191.
[43] T. R. Kirkpatrick and D. Thirumalai, J. Phys. A **22**, L149 (1989).
[44] T. R. Kirkpatrick and D. Thirumalai, Phys. Rev. A **37**, 4439 (1988).
[45] E. Flenner, M. Zhang, and G. Szamel, Phys. Rev. E **83**, 051501 (2011).
[46] E. Flenner and G. Szamel, Phys. Rev. Lett. **105**, 217801 (2010).
[47] M. D. Ediger, Annu. Rev. Phys. Chem. **51**, 99 (2000).
[48] G. Biroli and J. P. Garrahan, J. Chem. Phys. **138**, 12A301 (2013).
[49] R. Busch, W. Liu, and W. L. Johnson, J. Appl. Phys. **83**, 4134 (1998).
[50] H. W. Cho, M. L. Mugnai, T. R. Kirkpatrick, and D. Thirumalai, Phys. Rev. E **101**, 032605 (2020).
[51] C. A. Angell, Science **267**, 1924 (1995).